HHS Public Access

Author manuscript

Acta Histochem. Author manuscript; available in PMC 2023 June 30.

Published in final edited form as:

Acta Histochem. 2022 January ; 124(1): 151834. doi:10.1016/j.acthis.2021.151834.

Enhanced carbonic anhydrase expression with calcification and fibrosis in bronchial cartilage during COPD

Victor E. Nava[a], **Rahul Khosla**[b], **Samuel Shin**[c], **Federico E. Mordini**[d], **Bidhan C. Bandyopadhyay**[c,*]

[a]Pathology and Laboratory Medicine Service, Veterans Affairs Medical Center, 50 Irving Street, NW, Washington, DC 20422, USA

[b]Pulmonary Section, Medical Service, Veterans Affairs Medical Center, 50 Irving Street, NW, Washington, DC 20422, USA

[c]Calcium Signaling Laboratory, Research Service, Veterans Affairs Medical Center, 50 Irving Street, NW, Washington, DC 20422, USA

[d]Cardiology Section, Medical Service, Veterans Affairs Medical Center, 50 Irving Street, NW, Washington, DC 20422, USA

Abstract

Pulmonary cartilage plays a crucial structural role determining the physiologic airway compressibility and distensibility, necessary for proper mechanical function. This functionality deteriorates with aging due to increased stiffness of both airway muscle and cartilage, as well as, decreased renewal capacity. Altered airway remodeling has been suggested as a pathogenic driver of chronic obstructive pulmonary disease (COPD) through mechanisms still incompletely understood. Using paraffin-embedded lung tissue sections from archived autopsy material from COPD with non-COPD age matched controls a histopathologic analysis focused on inflammation, fibrosis and calcification was performed with special stains (Masson's trichrome and Von Kossa) and immunohistochemistry for carbonic anhydrase IV (CA IV) and Ki-67. COPD lung tissues showed increased peribronchial inflammation compared to the non-COPD. Coarse amphophilic

*Correspondence to: Calcium Signaling Laboratory, 151 Research Service, Veterans Affairs Medical Center, 50 Irving Street, NW, Washington, DC 20422, USA. bidhan.bandyopadhyay@va.gov (B.C. Bandyopadhyay).

Author contributions

Conception and design, acquisition and analysis (e.g., statistical analysis) of experimental data: V.E.N., S.S., R.K., F.E.M., and B.C.B.; Interpretation of data: B.C.B., V.E.N., S.S.; Writing the manuscript draft, review and revision of the manuscript: V.E.N., S.S., R.K., F.E.M., and B. C.B.; Funding acquisition: B.C.B. All authors have read and agreed to the submitted version of the manuscript.

Competing interest

There is no conflict of interest related to the submitted manuscript.

Ethical approval

Specimens are formalin fixed paraffin embedded (FFPE) de-identified tissue sections (biopsy sample, not individually identifiable to any person) from the Washington DC Department of Veterans Affairs Medical Center used through an exempt Institutional Review Board (IRB) protocol (protocol number: MIRB 01700; PI: BCB). This IRB exemption was also approved by the IRB and the Research and Development committee of the Washington DC VA Medical Center.

CRediT authorship contribution statement

Victor E. Nava: Conceptualization, Methodology, Writing – original draft, Writing – review & editing. **Rahul Khosla:** Data curation, Writing – original draft, Writing – review & editing. **Samuel Shin:** Software, Writing – original draft, Writing – review & editing. **Federico E. Mordini:** Writing – original draft, Writing – review & editing. **Bidhan C. Bandyopadhyay:** Conceptualization, Methodology, Visualization, Writing – review & editing.

crystalline deposits in bronchial cartilage were more frequently observed in COPD sections, which were compatible with early dystrophic calcification of the extracellular matrix and chondrocytes. Moreover, Von Kossa staining revealed a significant calcium deposition in the cartilages from COPD in comparison to the controls. Interestingly, Ki-67 immunostains demonstrated a higher overall proliferative rate, including epithelial cells, in COPD. Furthermore, Masson's trichrome staining revealed relatively increased peribronchial collagen deposition associated with a fibrotic stromal response, which may be secondary to the inflammatory milieu in COPD. To further characterize the tissue microenvironment associated with dystrophic calcification, immunohistochemistry for CA IV was used, revealing significantly increased expression in chondrocytes and peribronchial tissue in COPD. Our findings demonstrate that dystrophic calcification of the extracellular matrix and chondrocytes can be linked to CA IV expression in COPD and suggest that pH changes in pulmonary tissue associated with inflammation and calcification may play an active role in COPD.

Keywords

Lung cartilage; Chondrocyte; Turn over; Proliferation; Calcification; Chronic obstructive pulmonary disease (COPD); Carbonic anhydrase IV (CA IV); Tissue microenvironment

1. Introduction

Pulmonary calcification occurs in several systemic and pulmonary conditions and may be underrecognized because specific symptoms are often lacking (Chan et al., 2002). Calcification may be a marker of disease severity and chronicity. Pathophysiologic states predisposing to pulmonary calcification and ossification include hypercalcemia, a local alkaline environment, and previous lung injury (Chan et al., 2002). Enhanced alkaline phosphatase activity, active angiogenesis and growth factor mitogenic effects may also predispose to calcification. The clinical classification of pulmonary calcification includes both metastatic calcification (Brown et al., 1994; Mulligan, 1947), in which calcium accumulates in previously normal lung, and dystrophic calcification, which occurs in previously injured lung (Brown et al., 1994). Pulmonary ossification may be idiopathic or result from a variety of underlying pulmonary, cardiac or extra-cardiopulmonary disorders (Felson et al., 1984; Joines and Roggli, 1989; Kuplic et al., 1972). The diagnosis of pulmonary calcification/ossification requires various imaging techniques, such as chest radiography, computed tomographic scanning and bone scintigraphy (Felson et al., 1984; Joines and Roggli, 1989; Kuplic et al., 1972). Image analysis to detect and subclassify calcification/ossification may obviate the need for invasive biopsy. Various significant clinical conditions causing calcification/ossification in the lung include, chronic renal failure, orthotopic liver transplantation, granulomatous inflammation, DNAviral/parasitic infections, pulmonary amyloidosis, atherosclerosis and idiopathic pulmonary alveolar microlithiasis (Chan et al., 2002).

The C-shaped respiratory cartilage maintains patency of the respiratory tree by attaching to smooth muscle and connective tissue surrounding the airways. It has characteristic shapes and arrangements at different levels of the bronchi (Reid, 1976). The hyaline cartilage

present in the lung is dynamically remodeled and composed by chondrocytes that secrete extracellular matrix (ECM) rich in type II collagen and chondroitin sulfate. Chondrocytes receive mechanical, electrical and physicochemical signals transmitted by the ECM, and responds by regulating their metabolic activity (Huber et al., 2000; Goldring and Marcu, 2009). It has been suggested that respiratory cartilage plays an important active role in determining airway compressibility and distensibility. The mechanical function of the bronchial tree may be altered by age-related changes in rigidity of either the muscular or the cartilaginous component of the airways (Janssens et al., 1999; Shaffer et al., 2004; Sharma and Goodwin, 2006). However, the pathologic changes of respiratory cartilage related to chronic dyspnea have not been fully investigated yet.

Mature respiratory cartilage has a low metabolic activity, concordant with the decreased proliferative rate of adult chondrocytes, which may contribute to the age-related deterioration of the mechanical properties of cartilage (Huber et al., 2000; Martin and Buckwalter, 2001; Umlauf et al., 2010). Cell death and proliferation must be balanced in adult organisms in order to maintain homeostasis. Lung function remains steady from age 20–35 years and starts declining thereafter. Bronchial cartilage atrophy (diminished mass) has been implicated in the pathogenesis of chronic obstructive pulmonary disease (COPD) and other lung diseases, but its exact role remains controversial (San Jose Estepar et al., 2020; Maisel et al., 1972). Some reports indicate atrophic changes in bronchial cartilage may be most pronounced in emphysematous lungs (Wright, 1960; Thurlbeck et al., 1974). However, a quantitative study by Tandon and Campbell (Tandon and Campbell, 1969) also showed bronchial cartilage atrophy in chronic bronchitis. In contrast, two quantitative studies (Restrepo et al., 1964; Greenberg et al., 1967) showed no alteration of cartilage in the bronchi of patients with chronic bronchitis or emphysema. Similarly, studies have failed to demonstrate, reduction of bronchial cartilage volume in COPD patients (Maisel et al., 1972). Furthermore, two additional reports revealed no significant alteration in the amount of bronchial cartilage in asthma (Dunnill et al., 1969; Takizawa and Thurlbeck, 1971), and a recent study by Carroll et al. (1996) found no difference in amount of cartilage in the bronchi of patients who died from a rapid fatal attack of asthma versus those who died from long standing asthma. However, all these studies have been limited to a quantitative analysis of bronchial cartilage in COPD (chronic bronchitis and/or emphysema) or bronchial asthma, but none of them reported on histopathological changes. Therefore, to investigate histologic changes in lung tissue, which may be important to further understand the pathophysiology of COPD, we performed morphometric analyses of airways from autopsied patients, with a special reference to changes in bronchial cartilage.

2. Materials and methods

2.1. Tissue preparation

Specimens of formalin-fixed, paraffin-embedded (FFPE), de-identified lung tissue sections were obtained from archives of the Pathology and Laboratory Service at the Veterans Affairs Medical Center, Washington DC (VAMC). Permission to use the specimens for research was obtained from the Institutional Review Board Subcommittee and Research and Development Committee of VAMC and were limited to 3 consecutive years. We have reviewed a total

of twenty cases in which twelve were COPD and eight were non-COPD. Causes of death for COPD patients were sepsis secondary to cholecystitis and acute bronchopneumonia (3 patients). Non-COPD patients died of metastatic renal cell carcinoma (2 patients), adult T cell lymphoma/leukemia and invasive mammary duct carcinoma. All were males except one female with breast carcinoma. The ages ranged from 58 to 77 years (average 69) in the COPD group, and from 44 to 76 years (average 71) in the non-COPD group respectively.

To evaluate abnormalities associated to calcification/ossification of cartilages and determine histopathological signatures, samples with a significant amount of small airway cartilage were selected to allow special stains and immunohistochemistry. Antigen retrieval during immunohistochemistry caused occasional loss of cartilage impeding interpretation. Therefore, only tissues yielding entire full sections containing cartilage were further analyzed. This criterion resulted in a smaller sample size. Tissue blocks were cut into 5 micron sections and deparaffinized, which were then subjected to special stains and immunohistochemistry.

2.2. Special stains

Hematoxylin and eosin (H&E) stains were used for overall histologic assessment and to delineate inflammation and fibrosis. Sections were stained with the protocol and ready-to-use solutions obtained from Richard-Allan Scientific, Kalamazoo, MI. *Von Kossa Stain* was used to visualize calcium deposits, since it reacts specifically with calcium phosphate (Luna, 1968). *The Masson's trichrome method for connective tissue* (a triple stain) was used primarily to facilitate delineation of areas of collagen fibrosis, employing a Masson's Trichrome Stain Kit, Artisan™ (AR173) in an Artisan™ LinkPro Special Staining System autostainer (Dako, Carpenteria, CA). The three stains are Weigert's iron haematoxylin (nuclei, black), aniline blue (collagen fibers, blue) and Biebrish scarlet-acid fuchsin (all other tissue components, pink or red).

2.3. Immunohistochemistry (IHC)

2.3.1. IHC procedures—Standard immunohistochemical analysis was performed. In short, antibodies were localized as a brown precipitate via reaction with H_2O_2 and 3, 3 diaminobenzidine (DAB), using Envision and dual link HRP in a Dako Auto Stainer (Carpenteria, CA), and counterstained with hematoxylin. Native peroxidase was quenched in 3% H_2O_2. Reactions were enhanced by antigen retrieval in a pH buffer solution in a water bath. Cycling cell nuclei were labeled with monoclonal mouse anti-human antibodies to Ki-67 (Clone MIB-1, Agilent Technologies, Santa Clara, CA; Bai et al., 2013) to assess proliferative activity. A mouse monoclonal anti-human CA IV antibody [CA IV (E-6): sc-390371 from Santa Cruz Biotechnology, Inc., Dallas, TX] was used. The antibody dilution and reaction conditions were adjusted for optimal results (antibody dilution 1:50, 20 minand 15 min mouse linker, 20 min secondary antibody, 5 min DAB) in preliminary experiment with human colon and kidney tissue for positive controls. For negative controls, the primary antibody was replaced with a negative control cocktail of mouse IgG1, IgG2a, IgG2b, IgG3 and IgM. Criteria for optimal results included minimal background staining and cellular reactions with the appropriate distribution and intensity (Fleming et al., 1993).

2.4. Image quantification with ImageJ

Using digital photomicrographs of the slides obtained with a BX45 microscope (Olympus) and DP80 camera (Olympus), areas of calcification or fibrosis were quantified using the software ImageJ (National Institutes of Health). In order to increase the sampling while reducing the element of bias, images of 12 photomicrographs per case were taken from similar perichondrial locations from COPD and non-COPD (controls) samples. We then converted them to 8-bit black and gray images (when appropriate) to visualize calcification/fibrosis with special stains or immunoreactivity with antibodies (IHC). The program (ImageJ) summates the darkest areas of the photomicrograph, which coincide with the areas of positive staining. Based on these calculations, the total areas of calcification, inflammation, and fibrosis and DAB-immunoreactivity for CA IV, a relative score per section, were calculated from COPD and non-COPD groups. Fibrotic areas and degrees of fibrosis were estimated with a built-in "Threshold Color" tool in ImageJ as described (Yoon et al., 2020). Hue intervals for selecting different color gradient categories attributed with none, mild, moderate, and severe fibrosis, respectively. Similarly, Von Kossa and CA IV DAB-stained areas were estimated with a "Threshold" tool and particle analysis for pixel quantification of stained areas. Percentage of affected areas (calcified, fibrotic, or CA IV expressing) within tissue were assessed by dividing total area of tissue by total area of affected tissue and multiplied by 100. It must be emphasized, that this image manipulation generates an arbitrary scale to compare changes relative to the maximal intensity of the change observed, which does not necessarily correlate with the severity of the biological process or the possible peak of the process (fibrosis, calcification or CA IV expression) *in vivo*.

2.5. Proliferation

Ki-67-labeled and unlabeled cells were counted in the entire histologic section of comparable areas under 400X magnification using a Laboratory Counter (Clay-Adams, Parsnippany, NJ). The percent positive cells (*labeling index*) from each sample were determined, which was then analyzed in the COPD and non-COPD cases.

2.6. Statistical analysis

Data were expressed as mean ± standard error of the mean (SEM). Variance among three or more specimens in each COPD non-COPD groups was analyzed by a two-tailed *t*-test (Student t-distribution) using $P < 0.01$ or $P < 0.05$ for statistical significance.

3. Results

3.1. Inflammation and calcification in COPD lung tissue

Representative H&E-stained lung tissue sections of non-COPD patients were compared to that of COPD patients at 40x and 400x magnification (Fig. 1A–D). The expected increased chronic inflammatory infiltrates around airways and bronchial glands were seen in COPD, whereas little to no defined inflamed areas were observed in the non-COPD pulmonary control tissue (Fig. 1A–D). Of note, the inflammation was seen in peribronchial stroma and airway spaces, but not in the cartilage per se. In one case of COPD, prominent squamous

metaplasia was noted, as previously described in the literature. While most COPD cases showed variable peribronchial fibrosis, and bronchial gland enlargement (due to hyperplasia and hypertrophy) as seen in Fig. 1B, D, some cases also showed emphysematous changes. In COPD, the Reid index was higher than 0.4, which indicates that the linear distance between the airway epithelium and the plane of cartilage occupied by mucous glands is above 40% of the total distance between the epithelial surface and the cartilage. In addition, COPD patients showed increased frequency of blood-filled small vessels (high vessel tortuosity) in submucosal distribution compared with non-COPD patients, as has been documented previously. At low power the bronchial cartilage had a very similar appearance in COPD and non-COPD subjects. However, at higher magnifications, coarse amphophilic crystalline deposits in bronchial cartilage were more frequently observed in COPD vs. non-COPD controls (Fig. 1B, D), which were suggestive of early dystrophic calcification of the extracellular matrix. Non-COPD sections were for the most part unremarkable (Fig. 1A). One case had lymphomatous involvement by adult T cell leukemia/lymphoma but the uninvolved lung parenchyma showed no significant pathologic alterations.

3.2. Fibrosis in COPD lung tissue

Masson's tri-chrome-stained COPD pulmonary sections were compared to non-COPD controls to assess fibrosis (Fig. 2A–D). Significant perichondral and stromal collagen fibrosis (moderately darker blue) were detected in the COPD tissue when compared with controls (Fig. 2A–D), which was confirmed using a relative scale generated by ImageJ software, as described (Fig. 2E). Moreover, areas of moderate-severe fibrosis were prevalent in the COPD tissue compared to the non-COPD (Fig. 2E).

3.3. Cellular proliferation in COPD bronchial tissue

Proliferating cells in COPD lung tissue sections were identified by Ki-67 staining with a counter tool, and compared to non-COPD controls (Fig. 3A, B), as described. COPD sections revealed a significantly greater percentage of Ki-67-stained cells (including inflammatory and epithelial cells) in perichondrial fibrotic areas (Fig. 3C).

3.4. Cartilage calcification in COPD

Representative COPD lung tissue sections were stained with Von Kossa and compared to the non-COPD controls to confirm areas of suggestive of calcification (coarse amphophilic crystalline deposits) seen in H&E (Fig. 1). Cartilage from COPD lungs revealed increased areas of calcification (dark brown/black silver deposits) compared to the non-COPD control tissue on Von Kossa stains (Fig. 4A–D). ImageJ quantification demonstrated a significant difference (Fig. 4E). The calcific deposits were present predominantly in the ECM but also very close to chondrocytes (pericellular distribution).

3.5. Elevated expression of carbonic anhydrase (CA) IV in COPD lung tissue

CA is involved in diverse physiological and pathological processes, including respiration and transport of CO_2 and HCO_3- between metabolizing tissues and lungs (pH and CO_2 homeostasis). We found CA IV expression in all lung tissues examined; however, CA IV antibody staining (DAB reacting brown areas) was more prominent within the ECM

of cartilage in COPD compared to non-COPD tissue (Fig. 5A, B), which represented a significant increase when quantitated with ImageJ (Fig. 5C).

4. Discussion

We reviewed archived lung tissue samples from autopsy material from three consecutive years comparing COPD with non-COPD specimens to further study the pathology of the disease. Micromorphological examination revealed the expected increased chronic inflammatory infiltrates/fibrosis/bronchial gland enlargement that were associated with COPD, in comparison with the unremarkable control tissue (Fig. 1). Immunohistochemistry demonstrated lymphoid aggregates composed by a mixture of CD3-positive T cells, and less frequent CD20-positive B cells as described before (Wagner et al., 1998). Predictably, the non-COPD cases showed less overall chronic inflammation in peribronchial distribution. Although the proportion of T and B cells was similar between COPD and controls (data not shown). Immunohistochemistry for Ki-67 demonstrated a significantly higher proliferative rate (including epithelial cells) in COPD (Fig. 3). Epithelial linings were found intact in non-COPD compared to the COPD samples. Because an inflammatory milieu may induce a fibrotic stromal response (Zhan et al., 2017), staining of lung tissue was performed with Masson's trichrome, revealing increased peribronchial and parenchymal collagen deposition, as indicated by a significantly ($P < 0.05$) higher density of blue pigmentation of collagen (Fig. 2). Interestingly, a similar staining trend was observed in the ECM of cartilage, which showed darker blue staining when compared with non-COPD controls.

Unexpectedly, Von Kossa special stain confirmed increase calcium deposition (previously suggested by the H&E staining) in cartilage from COPD subjects (Fig. 4), which was statistically significant ($P < 0.01$) in comparison with non-COPD controls. Similar results were obtained with Alizarin Red staining (data not shown). The possibility that calcification was related to aging was eliminated in our study, since the average age of the COPD patients (68 yrs.) was higher than that of the non-COPD controls (64 yrs.).

Finally, immunohistochemistry for CA IV was attempted, where we lost many cartilage tissues during processing. Nonetheless, we have been able to analyze 12 COPD and 8 non-COPD cases, where we did enough sampling (average 12 pictures) to distinguish the differences. While we acknowledge the size limitation of our study; the observed differences between the COPD and non-COPD were very prominent. Future studies along this line can prospectively analyzed the lung biopsy samples to find the mechanism of such calcification associated CA IV expression. Interestingly, a markedly increased CA IV staining ($P < 0.01$) of chondrocytes and peribronchial tissue was detected in patients with COPD versus controls (Fig. 5). None of the COPD patients had elevated calcium levels or vitamin D levels in serum that could explain the observed calcification. One of the non-COPD patients had mildly elevated serum calcium (11.1 mg/dL), which was attributed to metastatic cholangiocarcinoma, since vitamin D and parathyroid hormone levels were normal. Notably, von Kossa stains did not demonstrate calcium deposition in lung cartilage of this patient, suggesting a COPD-specific mechanism. Furthermore, immunohistochemistry for CA IV was negative in this subject.

CA IV have been detected in pulmonary tissues on the luminal side of alveolar capillary endothelial cells, although its expression was absent in the large pulmonary vessels (Fleming et al., 1993). While the role of membrane bound CA IV in lung physiology has been studied using selective CA inhibitors, the results have been inconclusive (Esbaugh and Tufts, 2006), in part motivating this study. Current knowledge of the CA IV suggests that its selective expression in the alveolar capillaries implies that it can catalyze the dehydration of plasma bicarbonate (HCO_3^-) to carbon dioxide, which can diffuse across the capillary endothelial surface and be released during respiration (Waheed and Sly, 2014). While CA IV is cell membrane bound to the endothelium in lung, in renal epithelia it attaches to a phosphatidylinositol-glycan anchor (Zhu and Sly, 1990; Waheed and Zhu, 1992). We propose that the CA maintains a concerted effort with various Na^+, Cl^- and HCO_{3-} ion transporters to regulate ion and fluid movement and pH within the alveoli (Schwartz et al., 2000; Alvarez et al., 2003; Ohana, 2015). Pulmonary CA IV is similar to its renal counterpart with nearly identical properties, as well as being a “high activity” isozyme (Zhu and Sly, 1990). Furthermore, several studies have also examined CA IV as a potential biomarker for diseases, including appendicitis, myocardial infarction, or pancreatitis (Zamanova et al., 2019). Previous research has also shown that CAs are essential for calcification, especially for calcium bicarbonate formation (de Goeyse et al., 2021).

It is reasonable to hypothesize that the increased expression of CA IV during COPD allows the rise in conversion of HCO_{3-} to CO_2 and H_2O in the extracellular space, which are transported to the intracellular space. Subsequently, a cytosolic form of CA (CA II) would generate HCO_3^- intracellularly, which would then be utilized by the HCO_3^- transporter, NBCe1 (Lu et al., 2006), as part of a compensatory response to counter COPD-associated respiratory acidosis secondary to stable hypercapnia. The overexpression of CA IV in COPD would increase the acidity extracellularly, and the alkalinity intracellularly, which may promote calcification. Access of plasma HCO_{3-} to the large pool CA available in red blood cells makes pulmonary CA dispensable for CO_2 excretion. Another potential role proposed for pulmonary membrane-bound CA is to ensure complete plasma pH/pCO_2 equilibrium during capillary transit (Swenson et al., 1993). More simply, membrane-bound CA in the pulmonary capillaries would ensure that all chemical species are in complete equilibrium in plasma when blood leaves the lung. Accordingly, the main role of CA IV in the lung tissue, may be to indirectly regulate ventilation, via chemoreceptors in the peripheral and central nervous system that detect changes in acid-base chemical species (Lahiri and Forster, 2003). However, more thorough investigation is required to cement this mechanism, which is beyond the scope of our present study. In COPD, the main driver of hypoxemia includes ventilation/perfusion mismatch as a consequence of increased dead space due to decreased oxygen uptake related to alveolar damage or hypoventilation. Concomitant hypercapnia and compensatory tachypnea ensue. The observed increased CA IV expression in COPD, would also be present in hypoxemia, leading to a surge in HCO_3^- excretion to the extracellular space coupled with acidosis. In any case, CA has been shown to promote the formation of calcium carbonate (de Goeyse et al., 2021), intrinsic to calcification, although the exact mechanism of mineralization remains poorly understood (Liu et al., 2015). Nonetheless, upregulation of CA IV in calcified lung cartilage, as we report here in COPD, provides various opportunities for further research that may lead to

practical applications. Namely, exploring the possibility of using more sensitive imaging technology to detect microcalcifications in lung tissue in patients with COPD, which may be correlated with adverse prognosis, as has been shown with cardiovascular calcifications (Liu et al., 2015; Budoff et al., 2007), and spearheading investigations on the mechanisms of pH regulation linked to hypoxia.

Acknowledgments

We are thankful to Kathy A. Kalinyak and Lyvouch Filkoski, Pathology and Laboratory Service, VA Medical Center, Washington DC for technical help; and to Nhu Le and Madison Ezell (both Calcium Lab Research Students) for data analysis.

Funding

This study was supported in part by the Washington DC Department of Veterans Affairs Medical Center and by Pilot Translational and Clinical Studies (PTCS) program from Georgetown-Howard University Center for Clinical and Translational Science (GHUCCTS) to BCB. These funding sources were not involved in study design; collection, analysis, and interpretation of data; the writing of the manuscript; or in the decision to submit the article for publication.

Abbreviations:

CA IV,	carbonic anhydrase IV
COPD	chronic obstructive pulmonary disease
DAB	3, 3 diaminobenzidine
ECM	extracellular matrix
FFPE	formalin-fixed, paraffin-embedded
H&E	hematoxylin and eosin
HCO_3^-	bicarbonate
IHC	immunohistochemistry
NBCe1	sodium bicarbonate cotransporter 1
IgG	immunoglobulin G
SEM	standard error of the mean

References

Alvarez BV, Loiselle FB, Supuran CT, Schwartz GJ, Casey JR, 2003. Direct extracellular interaction between carbonic anhydrase IV and the human NBC1 sodium/bicarbonate co-transporter. Biochemistry 42 (42), 12321–12329. 10.1021/bi0353124. [PubMed: 14567693]

Bai X, Yan Y, Canfield S, Muravyeva MY, Kikuchi C, Zaja I, Corbett JA, Bosnjak ZJ, 2013. Ketamine enhances human neural stem cell proliferation and induces neuronal apoptosis via reactive oxygen species-mediated mitochondrial pathway. Anesth. Analg. 116 (4), 869–880. 10.1213/ANE.0b013e3182860fc9. [PubMed: 23460563]

Brown K, Mund DF, Aberle DR, Batra P, Young DA, 1994. Intrathoracic calcifications: radiographic features and differential diagnoses. Radio. Rev. Publ. Radio. Soc. N. Am. Inc. 14 (6), 1247–1261. 10.1148/radiographics.14.6.7855339.

Budoff MJ, Shaw LJ, Liu ST, Weinstein SR, Mosler TP, Tseng PH, Flores FR, Callister TQ, Raggi P, Berman DS, 2007. Long-term prognosis associated with coronary calcification: observations from a registry of 25,253 patients. J. Am. Coll. Cardiol. 49 (18), 1860–1870. 10.1016/j.jacc.2006.10.079. [PubMed: 17481445]

Carroll N, Carello S, Cooke C, James A, 1996. Airway structure and inflammatory cells in fatal attacks of asthma. Eur. Respir. J. 9 (4), 709–715. 10.1183/09031936.96.09040709. [PubMed: 8726935]

Chan ED, Morales DV, Welsh CH, McDermott MT, Schwarz MI, 2002. Calcium deposition with or without bone formation in the lung. Am. J. Respir. Crit. Care Med 165 (12), 1654–1669. 10.1164/rccm.2108054. [PubMed: 12070068]

Dunnill MS, Massarella GR, Anderson JA, 1969. A comparison of the quantitative anatomy of the bronchi in normal subjects, in status asthmaticus, in chronic bronchitis, and in emphysema. Thorax 24 (2), 176–179. 10.1136/thx.24.2.176. [PubMed: 5821620]

Esbaugh AJ, Tufts BL, 2006. The structure and function of carbonic anhydrase isozymes in the respiratory system of vertebrates. Respir. Physiol. Neurobiol. 154 (1–2), 185–198. 10.1016/j.resp.2006.03.007. [PubMed: 16679072]

Felson B, Schwarz J, Lukin RR, Hawkins HH, 1984. Idiopathic pulmonary ossification. Radiology 153 (2), 303–310. 10.1148/radiology.153.2.6435169. [PubMed: 6435169]

Fleming RE, Crouch EC, Ruzicka CA, Sly WS, 1993. Pulmonary carbonic anhydrase IV: developmental regulation and cell-specific expression in the capillary endothelium, 627–35 Dec;265(6 Pt 1):L627–35 Am. J. Physiol. 265. 10.1152/ajplung.1993.265.6.L627.

de Goeyse S, Webb AE, Reichart GJ, de Nooijer LJ, 2021. Carbonic anhydrase is involved in calcification by the benthic foraminifer Amphistegina lessonii. Biogeosciences 18 (2), 393–401. 10.5194/bg-18-393-2021.

Goldring MB, Marcu KB, 2009. Cartilage homeostasis in health and rheumatic diseases. Arthritis Res. Ther. 11 (3), 224. 10.1186/ar2592. [PubMed: 19519926]

Greenberg SD, Boushy SF, Jenkins DE, 1967. Chronic bronchitis and emphysema: correlation of pathologic findings. Am. Rev. Respir. Dis. 96 (5), 918–928. 10.1164/arrd.1967.96.5.918. [PubMed: 6059200]

Huber M, Trattnig S, Lintner F, 2000. Anatomy, biochemistry, and physiology of articular cartilage. Invest. Radio. 35 (10), 573–580. 10.1097/00004424-200010000-00003.

Janssens JP, Pache JC, Nicod LP, 1999. Physiological changes in respiratory function associated with ageing. Eur. Respir. J. 13 (1), 197–205. 10.1034/j.1399-3003.1999.13a36.x. [PubMed: 10836348]

Joines RW, Roggli VL, 1989. Dendriform pulmonary ossification. Report of two cases with unique findings. Am. J. Clin. Pathol. 91 (4), 398–402. 10.1093/ajcp/91.4.398.

Kuplic JB, Higley CS, Niewoehner DE, 1972. Pulmonary ossification associated with long-term busulfan therapy in chronic myeloid leukemia. Case report. Am. Rev. Respir. Dis. 106 (5), 759–762. 10.1164/arrd.1972.106.5.759. [PubMed: 4627906]

Lahiri S, Forster RE, 2003. CO2/H(+) sensing: peripheral and central chemoreception. Int. J. Biochem. Cell Biol. 35 (10), 1413–1435. 10.1016/s1357-2725(03)00050-5. [PubMed: 12818238]

Liu W, Zhang Y, Yu C-M, Ji QW, Cai M, Zhao YX, Zhou YJ, 2015. Current understanding of coronary artery calcification. J. Geriatr. Cardiol. JGC 12 (6), 668–675. 10.11909/j.issn.1671-5411.2015.06.012. [PubMed: 26788045]

Lu J, Daly CM, Parker MD, Gill HS, Piermarini PM, Pelletier MF, Boron WF, 2006. Effect of human carbonic anhydrase II on the activity of the human electrogenic Na/HCO3 cotransporter NBCe1-A in Xenopus oocytes. J. Biol. Chem. 281 (28), 19241–19250. 10.1074/jbc.M602181200. [PubMed: 16687407]

Luna LG, 1968. Manual of Histologic Staining Methods of the Armed Forces Institute of Pathology.. McGraw–Hill, New York, pp. 174–188.

Maisel JC, Silvers GW, George MS, Dart GA, Petty TL, Mitchell RS, 1972. The significance of bronchial atrophy. Am. J. Pathol. 67 (2), 371–386. [PubMed: 5021107]

Martin JA, Buckwalter JA, 2001. Roles of articular cartilage aging and chondrocyte senescence in the pathogenesis of osteoarthritis. Iowa Orthop. J. 21, 1–7. [PubMed: 11813939]

Mulligan RM, 1947. Metastatic calcification. Arch. Pathol. 43 (2), 177–230.

Ohana E, 2015. Transepithelial ion transport across duct cells of the salivary gland. Oral. Dis. 21 (7), 826–835. 10.1111/odi.12201. [PubMed: 24164806]

Reid L, 1976. Visceral cartilage. J. Anat. 122 (Pt 2), 349–355. [PubMed: 794047]

Restrepo GL, Heard BE, 1964. Air trapping in chronic bronchitis and emphysema: measurements of the bronchial cartilage. Am. Rev. Respir. Dis. 90, 395–400. 10.1164/arrd.1964.90.3.395. [PubMed: 14215908]

San Jose Estepar R, Nardelli P, Diaz A, Washko GR, 2020. Bronchial cartilage loss is associated with small airway disease but not emphysema. In: D28. COPD: FROM PATHOGENESIS TO PROGNOSIS. American Thoracic Society International Conference Abstracts. American Thoracic Society, A6416–A6416. doi:10.1164/ajrccm-conference.2020.201.1_MeetingAbstracts.A6416.

Schwartz GJ, Kittelberger AM, Barnhart DA, Vijayakumar S, 2000. Carbonic anhydrase IV is expressed in H(+)-secreting cells of rabbit kidney. Am. J. Physiol. Ren. Physiol. 278 (6), F894–F904. 10.1152/ajprenal.2000.278.6.F894.

Shaffer TH, Wolfson MR, Panitch HB, 2004. Airway structure, function and development in health and disease. Paediatr. Anaesth. 14 (1), 3–14. 10.1046/j.1460-9592.2003.01207.x. [PubMed: 14717868]

Sharma G, Goodwin J, 2006. Effect of aging on respiratory system physiology and immunology. Clin. Inter. Aging 1 (3), 253–260. 10.2147/ciia.2006.1.3.253.

Swenson ER, Robertson HT, Hlastala MP, 1993. Effects of carbonic anhydrase inhibition on ventilation-perfusion matching in the dog lung. J. Clin. Invest. 92 (2), 702–709. 10.1172/JCI116640. [PubMed: 8349809]

Takizawa T, Thurlbeck WM, 1971. Muscle and mucous gland size in the major bronchi of patients with chronic bronchitis, asthma, and asthmatic bronchitis. Am. Rev. Respir. Dis. 104 (3), 331–336. 10.1164/arrd.1971.104.3.331. [PubMed: 5098669]

Tandon MK, Campbell AH, 1969. Bronchial cartilage in chronic bronchitis. Thorax 24 (5), 607–612. 10.1136/thx.24.5.607. [PubMed: 5348329]

Thurlbeck WM, Pun R, Toth J, Frazer RG, 1974. Bronchial cartilage in chronic obstructive lung disease. Am. Rev. Respir. Dis. 109 (1), 73–80. 10.1164/arrd.1974.109.1.73. [PubMed: 4809167]

Umlauf D, Frank S, Pap T, Bertrand J, 2010. Cartilage biology, pathology, and repair. Cell Mol. Life Sci. CMLS 67 (24), 4197–4211. 10.1007/s00018-010-0498-0. [PubMed: 20734104]

Wagner UG, Kurtin PJ, Wahner A, Brackertz M, Berry DJ, Goronzy JJ, Weyand CM, 1998. The role of CD8+ CD40L+ T cells in the formation of germinal centers in rheumatoid synovitis. J. Immunol. 161 (11), 6390–6397. [PubMed: 9834130]

Waheed A, Sly WS, 2014. Membrane associated carbonic anhydrase IV (CA IV): a personal and historical perspective. Subcell. Biochem. 75, 157–179. 10.1007/978-94-007-7359-2_9. [PubMed: 24146379]

Waheed A, Zhu XL, 1992. Sly WS. Membrane-associated carbonic anhydrase from rat lung. Purification, characterization, tissue distribution, and comparison with carbonic anhydrase IVs of other mammals. J. Biol. Chem. 267 (5), 3308–3311. [PubMed: 1737787]

Wright RR, 1960. Bronchial atrophy and collapse in chronic obstructive pulmonary emphysema. Am. J. Pathol. 37, 63–77. [PubMed: 13846107]

Yoon H, Lee YS, Lim BJ, Han K, Shin HJ, Kim MJ, Lee MJ, 2020. Renal elasticity and perfusion changes associated with fibrosis on ultrasonography in a rabbit model of obstructive uropathy. Eur. Radiol. 30 (4), 1986–1996. 10.1007/s00330-019-06547-4. [PubMed: 31858205]

Zamanova S, Shabana AM, Mondal UK, Ilies MA, 2019. Carbonic anhydrases as disease markers. Expert Opin. Ther. Pat. 29 (7), 509–533. 10.1080/13543776.2019.1629419. [PubMed: 31172829]

Zhan H-X, Zhou B, Cheng Y-G, Xu JW, Wang L, Zhang GY, Hu SY, 2017. Crosstalk between stromal cells and cancer cells in pancreatic cancer: new insights into stromal biology. Cancer Lett. 392, 83–93. 10.1016/j.canlet.2017.01.041. [PubMed: 28189533]

Zhu XL, Sly WS, 1990. Carbonic anhydrase IV from human lung. Purification, characterization, and comparison with membrane carbonic anhydrase from human kidney. J. Biol. Chem. 265 (15), 8795–8801. [PubMed: 2111324]

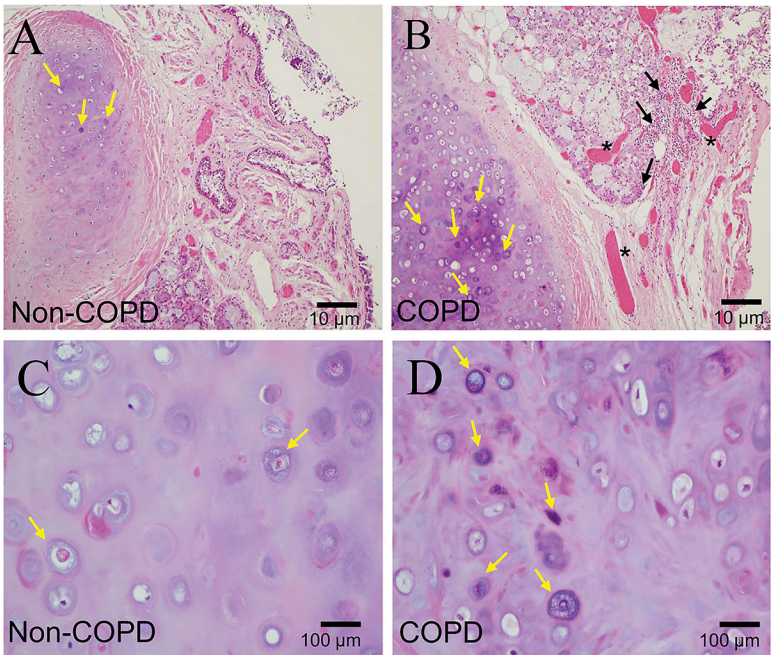

Fig. 1.

H&E staining of non-COPD (A, C) and COPD (B, D) lung tissue sections. Coarse basophilic deposits (yellow arrows) in extracellular matrix in COPD tissue, suggestive of early calcification. Black arrows and star symbols indicate chronic inflammation and tortuous blood vessels, respectively.

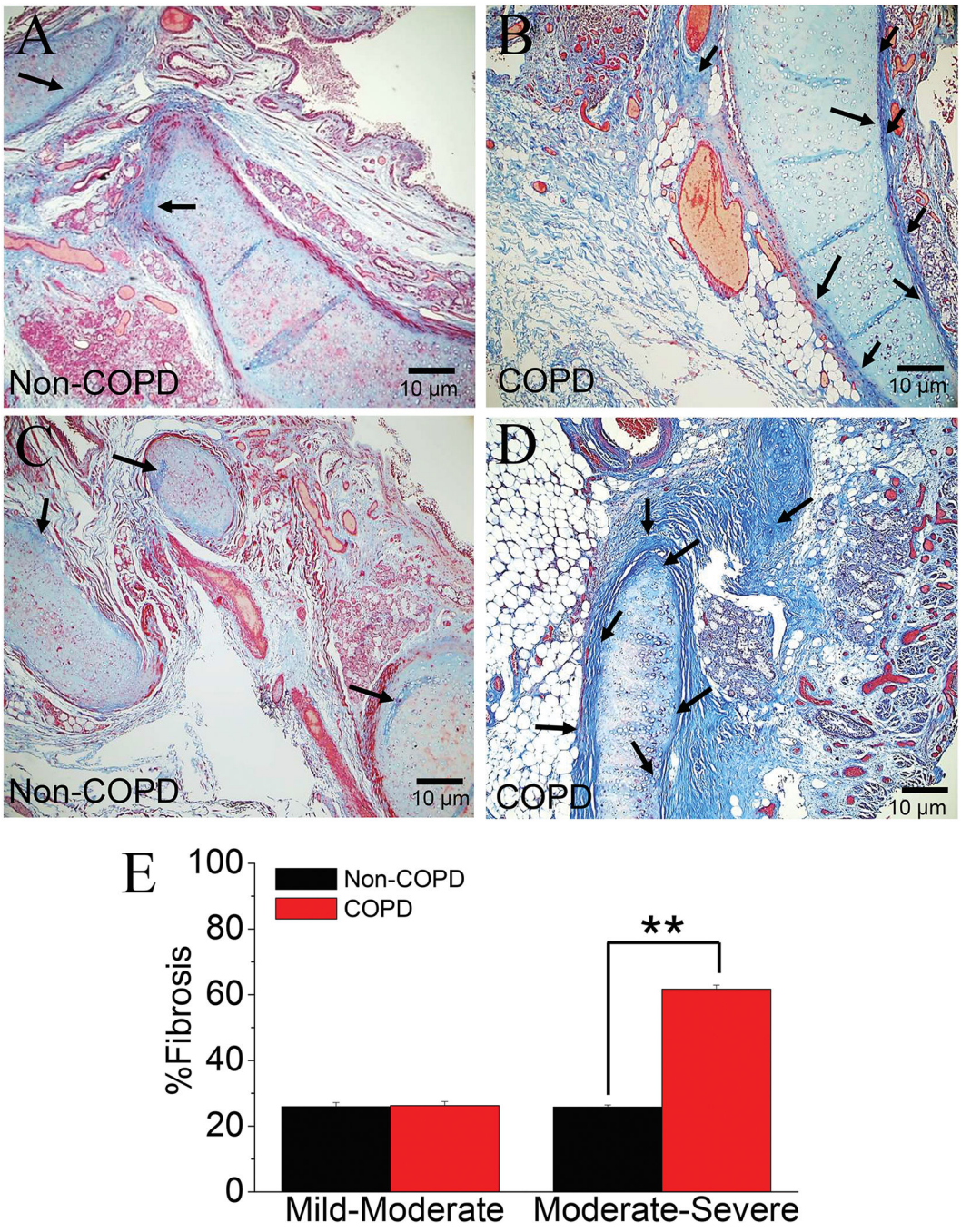

Fig. 2.

Masson's trichrome staining of non-COPD (A, C) and COPD (B, D) lung tissue sections (40x magnification). Arrows depict fibrotic regions in both non-COPD and COPD tissue, which are significantly increased (** $P < 0.01$) in COPD tissue, as indicated by darker blue staining, in COPD. Bar diagram represents degree of fibrosis from non-COPD and COPD sections with ImageJ quantification (E).

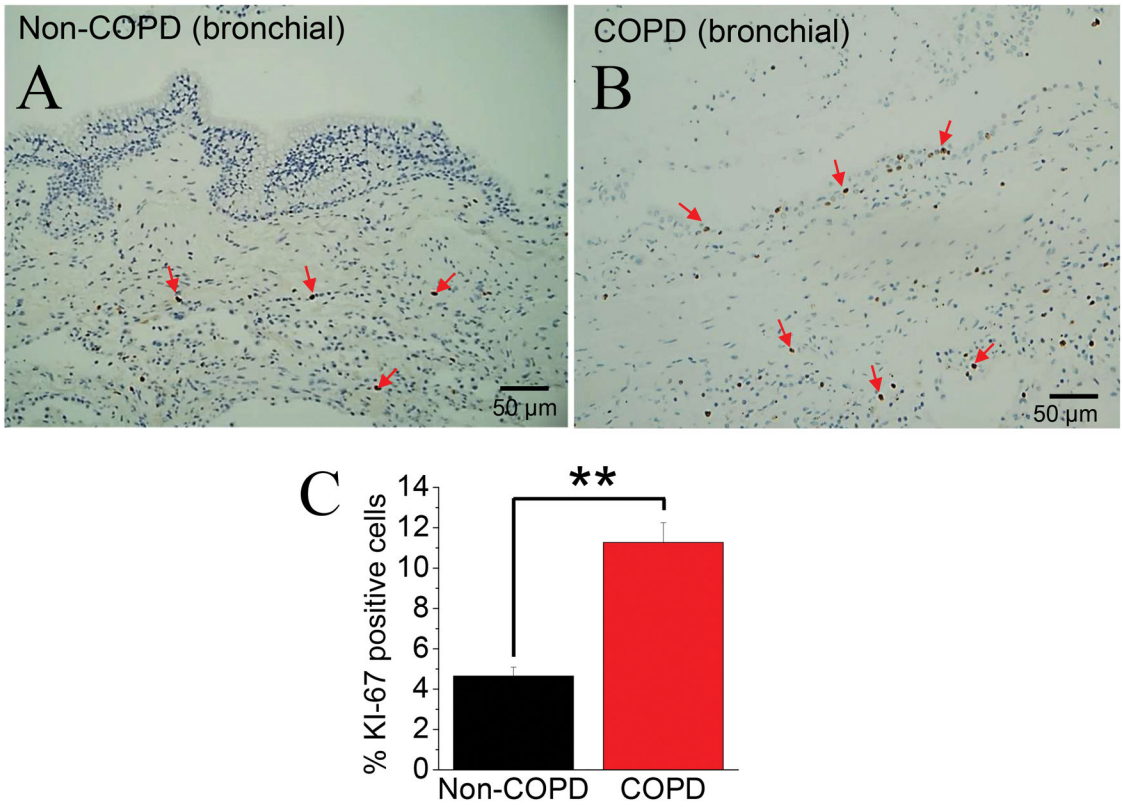

Fig. 3.

Ki-67 immunostaining of non-COPD (A) and COPD (B) lung tissue sections (200x magnification). Increased proliferation index (inflammatory and epithelial cells) in perichondral fibrotic areas of COPD lung tissue shown (red arrows). Arrows depict stained cells undergoing proliferation. Bar diagrams summarize percentage of Ki-67 positive cells in non-COPD and COPD sections as quantitated by ImageJ software (C). (* $P < 0.05$).

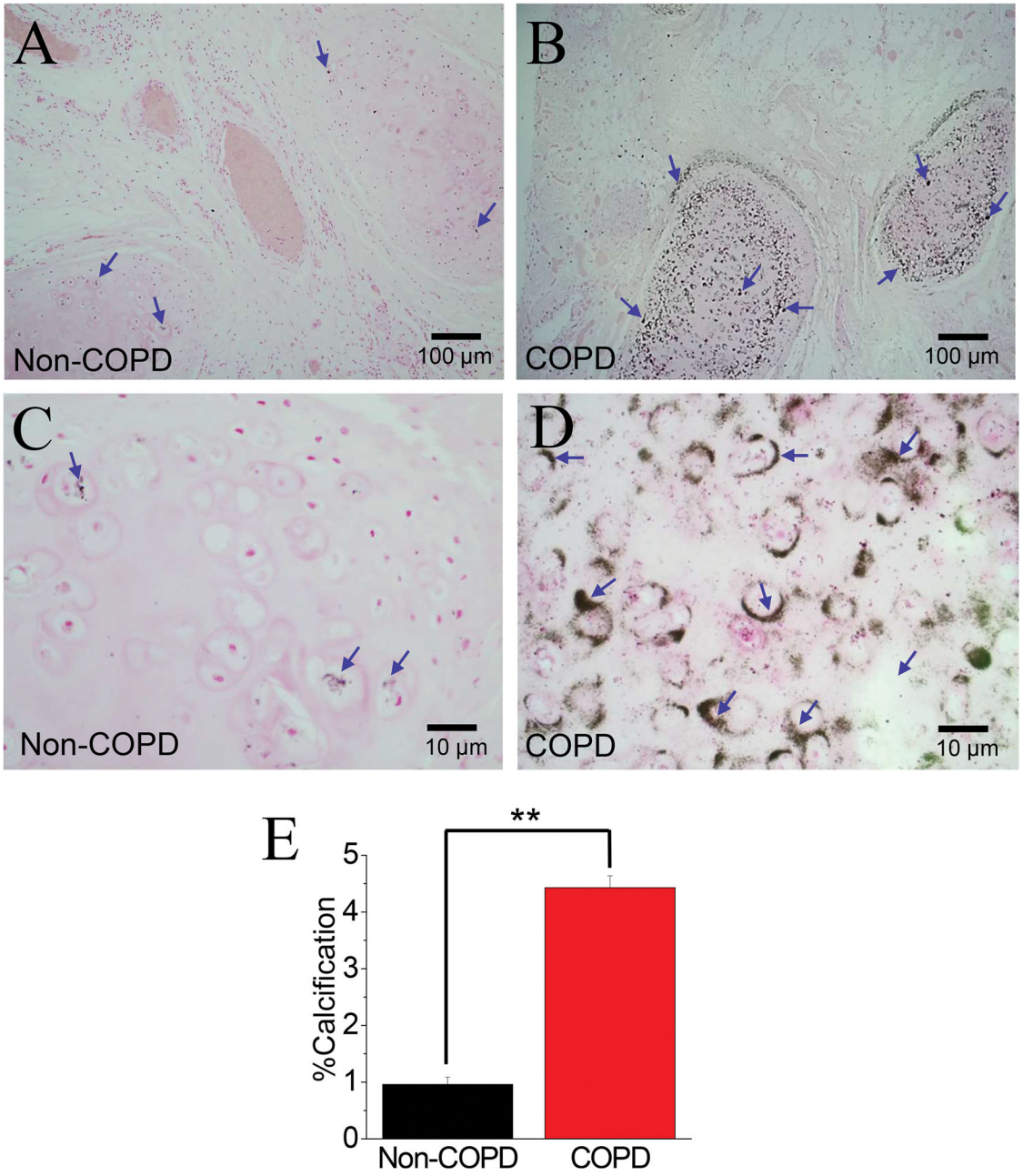

Fig. 4.

Von Kossa staining of non-COPD (A, C) and COPD (B, D) lung tissue sections (40x and 400x magnification). Blue arrows depict areas of calcification, indicated by Von Kossa staining. Bar diagrams summarizing percentage of Von Kossa staining in non-COPD and COPD sections as quantitated by ImageJ software (E). (** $P < 0.01$).

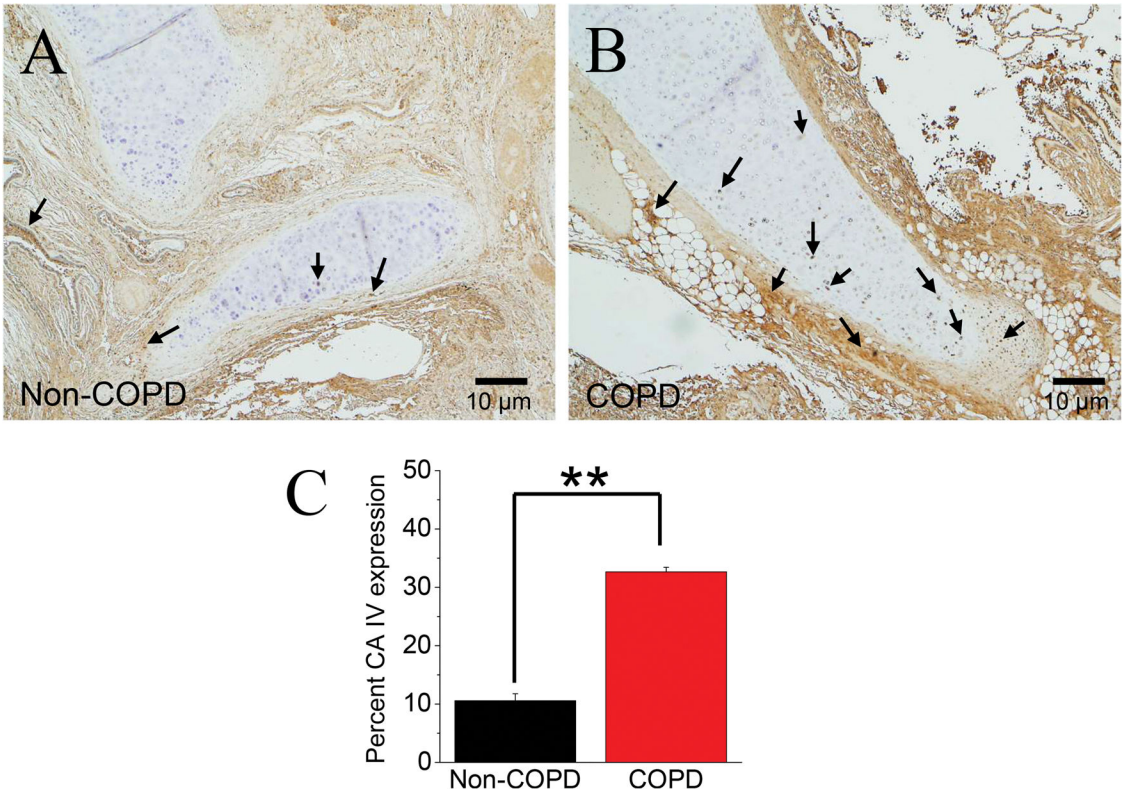

Fig. 5.

Immunohistochemistry of CA IV localization depicted by DAB staining (brown precipitate) in non-COPD (A) and COPD (B) lung tissue (40x magnification). Black arrows depict regions of CA IV localization by DAB staining. Bar diagrams summarizing percentage DAB staining in non-COPD and COPD sections as quantitated by ImageJ software (C). (** $P < 0.01$)